Vortex pinning by meandering line defects in planar superconductors

Eleni Katifori* and David R. Nelson
Department of Physics, Harvard University, Cambridge, Massachusetts 02138, USA
(Received 10 January 2006; revised manuscript received 24 April 2006; published 6 June 2006)

To better understand vortex pinning in thin superconducting slabs, we study the interaction of a single fluctuating vortex filament with a curved line defect in $(1+1)$ dimensions. This problem is also relevant to the interaction of scratches with wandering step edges in vicinal surfaces. The equilibrium probability density for a fluctuating line attracted to a particular fixed defect trajectory is derived analytically by mapping the problem to a straight line defect in the presence of a space and time-varying external tilt field. The consequences of both rapid and slow changes in the frozen defect trajectory, as well as finite size effects are discussed. A sudden change in the defect direction leads to a delocalization transition, accompanied by a divergence in the trapping length, near a critical angle.

DOI: 10.1103/PhysRevB.73.214503 PACS number(s): 74.25.Qt, 72.15.Rn

I. INTRODUCTION

Understanding the physics of thermally wandering lines interacting with extended defects is crucial in explaining the properties of planar high-T_c superconductors permeated by columnar pins or twin boundaries.[1] Considerable progress is possible theoretically in planar superconductors, when platelet samples are permeated by a single sheet of vortex lines due to a small in-plane magnetic field.[2,3] Related problems arise on vicinal surfaces, where thermally fluctuating step edges[4] can interact with scratches, grain boundaries or terraces created by lithography. In superconductors, a zoo of different systems whose properties are determined by the interplay of the interacting vortex filaments, thermal fluctuations and pinning has been thoroughly explored when the attracting defect is straight or vortices follow trajectories determined by point disorder.[1,2,5–8] However, little work has been done so far when the defects themselves follow a controlled but nontrivial trajectory. On vicinal surfaces, such defects could be created by etching a wavy, semipermanent scratch, or studied in the context of the square terraces created lithographically by Lee and Blakely.[9] One might also consider a thin high-T_c superconductor sample where a wavy notch has been etched, although curved extended defects can arise naturally in the form of grain boundaries in polycrystalline platelet superconductors.[15] Finally, close intersection of splayed columnar defects[10,11] provide preferred vortex tracks with a sudden change of direction.

In this work we investigate a single thermally fluctuating line that interacts with a single quenched meandering defect. This situation mimics the dilute flux line limit of a planar superconductor with a single pinning defect when the vortices are far apart enough to be considered noninteracting. Although we use the terminology of flux lines throughout, similar results should apply to scratch-step interactions on vicinal surfaces. The more complicated many body problem of many step edges (or vortex lines) interacting with a single curved line defect and with each other will be treated in a future publication.[16]

In the spirit of the treatment of high-T_c superconductors in Ref. 5, we describe the trajectory of a flux line in $(1+1)$ dimensions as a classical elastic string $x(\tau)$ subject to thermal fluctuations. We assume high enough temperatures and sufficiently clean samples so that point disorder can be neglected. In a quantum analogy[2,3] (see below) the spatial direction labeled by τ plays the role of imaginary time. We assume that overhangs are improbable, so the choice of a single valued function to describe a stringlike flux line is adequate. The trajectory of the defect itself (a notch, etched on the thin superconducting slab, say) will be represented as $x_0(\tau)$, and attracts the vortex with a short range attractive potential $V[x-x_0(\tau)]$, (see Fig. 1).

For the energy of a flux line induced by a magnetic field along τ in $(1+1)$ dimensions, bounded by timelike initial and final coordinates τ_i and τ_f, we take the integral

$$E[x(\tau)] = \int_{\tau_i}^{\tau_f} d\tau \left[\frac{\gamma}{2} \left(\frac{dx(\tau)}{d\tau} \right)^2 + V[x(\tau) - x_0(\tau)] \right], \quad (1)$$

where γ is the coarse-grained line tension. The finite temperature behavior of the string can be determined from the partition function, which is a functional integral over all possible vortex configurations $x(\tau)$,

$$\mathcal{Z} = \int \mathcal{D}x(\tau) e^{-E[x(\tau)]/T}, \quad (2)$$

where we have set Boltzmann's constant $k_B \equiv 1$.

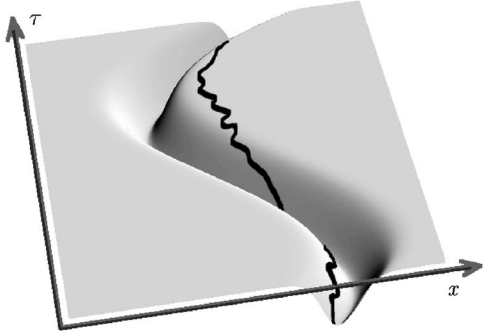

FIG. 1. Thermally excited fluctuating string (vortex line or step edge) interacting with a meandering attractive linelike potential. The dark line indicates the elastic string trajectory $x(\tau)$, the energy of which is given by Eq. (1).

The statistical physics of the above system is controlled by a competition between the two terms of the line energy of Eq. (1). The "kinetic energy" (corresponding to the line tension of the string) is minimized when the vortex line is straight and parallel to the τ direction, whereas the "potential energy" is minimized when the string resides at the deepest point of $V[x(\tau)-x_0(\tau)]$, namely, exactly on the attracting defect. Depending on the strength of the potential, the stiffness of the string, the temperature and the trajectory $x_0(\tau)$ of the defect, the elastic string will either localize near the trajectory of the defect or wander far from it. Since in most experimental realizations the attractive potential is relatively short ranged, in this work we will take $V[x]$ in Eq. (1) to be an attractive delta function, which should adequately describe the long wavelength properties of the system.

The case of $x_0(\tau)$ being a zeroth or first order polynomial of τ (i.e., a straight line!) has been studied in detail in Ref. 5, with emphasis on the delocalization transition that takes place for large relative tilts of the pinning defect and the flux line. This work adapts the results and conclusions of that paper to the case of a "bent defect" with a sudden change in direction, and considers more general quenched defect trajectories as well.

This paper will be structured as follows. In Sec. II we review the basic mapping from a classical description of the thermally fluctuating flux line to a (non-Hermitian) quantum mechanical problem, and use this mapping to analytically compute the partition function (i.e., the propagator for the equivalent quantum problem) for the straight defect case. Section III explains how to use this propagator to derive exact expressions for a simple realization of a "bent" defect trajectory and determine how the defect probability distribution responds to the presence of the kink. Section IV describes a perturbative solution in the "Born-Oppenheimer" limit of a slowly varying $x_0(\tau)$. In Sec. V we give a brief summary of this paper's conclusions and suggest some possible experiments that could be done to test them. Finally, the Appendix contains some calculational details, relevant to Secs. II and III.

II. PARTITION FUNCTION FOR A FLUX LINE INTERACTING WITH A LINEAR DEFECT

In this section we briefly review the connection between the classical path integral of Eq. (2) and the "quantum mechanical" formulation, which follows from a transfer matrix technique.[12] We then proceed to analytically compute the partition function that governs the properties of the thermally excited vortex line interacting with a straight line defect.

For clarity we denote the partition function of Eq. (2) as $\mathcal{Z}[x_f,\tau_f;x_i,\tau_i;x_0(\tau)]$, where x_i and x_f are fixed initial and final positions of the flux line. (We may eventually choose to integrate over these endpoints.) Since the potential is only implicitly dependent on τ through the defect coordinate $x_0(\tau)$, we can map the problem by a change of variables $x(\tau)\rightarrow y(\tau)=x(\tau)-x_0(\tau)$ onto one of a straight defect in a τ-dependent external tilt field $h(\tau)=dx_0(\tau)/d\tau$ that imposes tendency to drift on the flux line. The Jacobian of the transformation is unity, so the measure of the path integral remains the same. After this transformation, the partition function reads

$$\mathcal{Z}_t[x_f-x_0(\tau_f),\tau_f;x_i-x_0(\tau_i),\tau_i;h(\tau)]=\int \mathcal{D}y(\tau)e^{-E[y(\tau)]/T}, \tag{3}$$

where

$$E[y(\tau)]=\int_{\tau_i}^{\tau_f}d\tau\left[\frac{\gamma}{2}\left(\frac{dy(\tau)}{d\tau}+h(\tau)\right)^2-V_0\delta(y)\right]. \tag{4}$$

The sign of $V_0>0$ is chosen so that the potential is attractive. By construction, the old and new partition functions must agree:

$$\mathcal{Z}[x_f,\tau_f;x_i,\tau_i;x_0(\tau)]=\mathcal{Z}_t[x_f-x_0(\tau_f),\tau_f;x_i-x_0(\tau_i),\tau_i;h(\tau)]. \tag{5}$$

One way around the technical difficulties (see, e.g., Ref. 13) of the evaluation of the partition function of Eq. (3) due to the singular nature of the delta function, is to recast the problem in quantum language. The classical partition function then becomes a matrix element of the imaginary time evolution operator

$$\mathcal{Z}_t[x_f,\tau_f;x_i,\tau_i;h(\tau)]=\langle x_f|T_\tau\{e^{-\int_{\tau_i}^{\tau_f}d\tau\,\mathcal{H}(\tau)/T}\}|x_i\rangle, \tag{6}$$

where the time ordering operator T_τ is required by the time-dependent Hamiltonian

$$\mathcal{H}(\tau)=-\frac{T^2}{2\gamma}\frac{\partial^2}{\partial x^2}-h(\tau)T\frac{\partial}{\partial x}-V_0\delta(x). \tag{7}$$

The mapping onto imaginary time quantum mechanics is clear if we let $T\rightarrow\hbar$ and $\gamma\rightarrow m$, where m is a particle mass. The term $h(\tau)T\frac{\partial}{\partial x}$ makes the Hamiltonian non-Hermitian.

Before considering curved defect trajectories, we analytically compute the matrix element $\mathcal{Z}_t[x,\tau;y,0;h]$ for constant tilt h, by expanding with respect to the complete set of right and left energy eigenstates $\{|\psi_K\rangle_R\}$ and $\{{}_L\langle\psi_K|\}$ of the non-Hermitian Hamiltonian of Eq. (7):

$$\mathcal{Z}_t[x,\tau;y,0;h]=\sum_K \langle x|\psi_K\rangle_R e^{-E_K\tau/T}{}_L\langle\psi_K|y\rangle, \tag{8}$$

with E_K being the Kth eigenenergy. Since both the Hamiltonian and the propagator are τ-translationally invariant, without loss of generality we have chosen zero as the origin of imaginary time. For notational simplicity we have also rescaled the spatial coordinates (x,τ) and tilt h so that $[x]=T^2/\gamma V_0$, $[\tau]=2T^3/\gamma V_0^2$, $[h]=V_0/T$. After these rescalings, the evolution equation for $\mathcal{Z}_t[x,\tau;x_i,\tau_i;h]\equiv\mathcal{Z}[x,\tau]$ reads

$$\frac{\partial\mathcal{Z}[x,\tau]}{\partial\tau}=-\mathcal{H}\mathcal{Z}[x,\tau]=\left(\frac{\partial^2}{\partial x^2}+2h(\tau)\frac{\partial}{\partial x}+2\delta(x)\right)\mathcal{Z}[x,\tau]. \tag{9}$$

As explained in Ref. 5, there is a critical value h_c of the tilt, above which the flux line delocalizes from the defect. Our rescaled units are chosen so that this value is $h_c=1$ for our delta function potential. Notice that in the rescaled units the

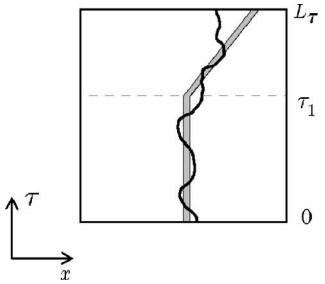

FIG. 2. Flux line near a kinked defect. The defect, initially parallel to the average direction of the freely fluctuating vortex suddenly tilts at $\tau=\tau_1$.

track of the straight line defect is given by $dx_0(\tau)/dt=2h$.

The set of normalizable eigenstates of Eq. (7) is different above and below the critical tilt h_c (see the Appendix); however, the propagator when the lateral dimension L_x of the sample tends to infinity has the same form for both regimes, namely,

$$\mathcal{Z}_t[x,\tau;y,0;h]=e^{-h(x-y)-h^2\tau}\left[\frac{e^{-(x-y)^2/4\tau}}{2\sqrt{\pi\tau}}+\frac{e^{-|y|-|x|+\tau}}{2}\mathrm{erfc}\left(\frac{|y|+|x|}{2\sqrt{\tau}}-\sqrt{\tau}\right)\right], \quad (10)$$

where $\mathrm{erfc}(x)=\frac{2}{\sqrt{\pi}}\int_x^\infty dt e^{-t^2}$. The first term inside the square brackets is independent of the defect, translationally invariant in the x direction and describes the random thermal "diffusion with drift" of the flux line $\mathcal{Z}\sim\exp[-(x+2h\tau)^2/4\tau]$.[17] This term dominates for small times and/or large $|x|$, $|y|$, i.e., far from the defect. The second term becomes important for sufficiently large imaginary times or small $|x|$, $|y|$. The delocalization transition manifests itself in the exponential growth of the second term for large $|x|$, $|y|$ when the tilt h in the prefactor exceeds the critical tilt $h_c=1$. Upon returning to the original units of x and τ, we see that the effect of the defect becomes apparent for $\tau>\tau_c^*\simeq T^3/\gamma V_0^2$, provided $|x|$ and $|y|$ are within a localization length $x^*=T^2/\gamma V_0$ of the defect at the origin. For $V_0\to 0$, the first term in the brackets scales as $1/V_0$ and will dominate over the second term which becomes independent of V_0. This limit leads to the expected free flux line propagator. These results can be easily translated in the original frame of reference (where the defect is tilted) by the use of Eq. (5).

III. PROBABILITY DISTRIBUTION OF THE FLUCTUATING VORTEX FILAMENT

In this section we use the above propagator to analytically compute the probability distribution function of a flux line interacting with a τ-dependent defect. As a simple, yet revealing example we study a line defect consisting of two straight lines joined at an angle, at $\tau=\tau_1$, namely, $x_0(\tau)=2h(\tau-\tau_1)\Theta(\tau-\tau_1)$, see Fig. 2. Here, $\Theta(x)$ is the step function, $\Theta(x)=0$, $x<0$, $\Theta(x)=1$, $x>0$. Any sufficiently well behaved defect trajectory can be approximated by a series of finite segments; the method described below can be straightforwardly generalized to more complicated piecewise linear configurations.

When $h<1$, and in particular when $h=0$ for the first segment of the defect, the system relaxes to the localized ground state exponentially fast as τ becomes large. A ground state initial condition $|\psi^i\rangle=|\psi_g\rangle$ at $\tau=0$ is thus the experimentally relevant case when the kink at τ_1 is sufficiently far from the boundaries. For $\tau=L_\tau$ we choose free boundary conditions embodied in the final state $\langle\psi^f|=\int dy\langle y|$, meaning that no restriction is imposed on the exit point of the vortex from the sample. In what follows, unless otherwise stated, we work in the thermodynamic limit in the x direction, so integrations such as $\int dx$ may be understood as $\int_{-\infty}^{\infty}dx$.

The probability distribution for the flux line on some internal time slice τ is formally equal to

$$P(x,\tau)=\frac{1}{\mathcal{Z}}\langle\psi^f|S(L_\tau,\tau)|x\rangle\langle x|S(\tau,0)|\psi^i\rangle, \quad (11)$$

where

$$S(\tau_f,\tau_i)\equiv T_\tau\{e^{-\int_{\tau_i}^{\tau_f}d\tau\,\mathcal{H}(\tau)/T}\} \quad (12)$$

is the time ordered evolution operator associated with the Hamiltonian

$$\mathcal{H}(\tau)=-\frac{T^2}{2\gamma}\frac{\partial^2}{\partial x^2}-V_0\delta[x-x_0(\tau)]. \quad (13)$$

In Eq. (11), $\mathcal{Z}$ is used to represent the partition function for the entire length of the system on both sides of the kink

$$\mathcal{Z}\equiv\langle\psi^f|S(L_\tau,0)|\psi^i\rangle. \quad (14)$$

Since the defect trajectory $x_0(\tau)$ is piecewise straight, we can split the factors in the numerator of Eq. (11) into two pieces such that $dx_0/d\tau=$const. For computational purposes, the cases $\tau>\tau_1$ and $\tau<\tau_1$ need to be treated separately.

First, for $\tau<\tau_1$ we expand the probability distribution in position eigenstates as

$$\begin{aligned}P(x,\tau)&=\frac{1}{\mathcal{Z}}\int\int \mathrm{d}y\mathrm{d}y'\langle y|S(L_\tau,\tau_1)|y'\rangle\langle y'|S(\tau_1,\tau)|x\rangle\\&\quad\times\langle x|S(\tau,0)|\psi_g\rangle\\&=\frac{1}{\mathcal{Z}}\int\int \mathrm{d}y\mathrm{d}y'\,\mathcal{Z}[y,L_\tau;y',\tau_1;x_0(\tau)]\mathcal{Z}[y',\tau_1;x,\tau;0]\\&\quad\times\langle x|S(\tau,0)|\psi_g\rangle. \quad (15)\end{aligned}$$

The last propagator inside the integrand effectively localizes the vortex near the defect at $x_0(\tau)=0$ case. Since the initial condition is the ground state of the time independent Hamiltonian, this last factor is just equal to $e^{-|x|}e^{-E_g\tau}=e^{-|x|}e^{\tau}$, since the ground state energy in our units is $E_g=-1$. The middle propagator in Eq. (15) follows from Eq. (10) by setting $h=0$. The leftmost factor in the integrand can also be expressed in terms of Eq. (10), if we first perform the transformation of Eq. (5). Then, since y' is a dummy integration variable and $x_0(\tau_1)=0$, it is easy to see that Eq. (15) can be rewritten in terms of the transformed partition function appearing in Eq. (5) as

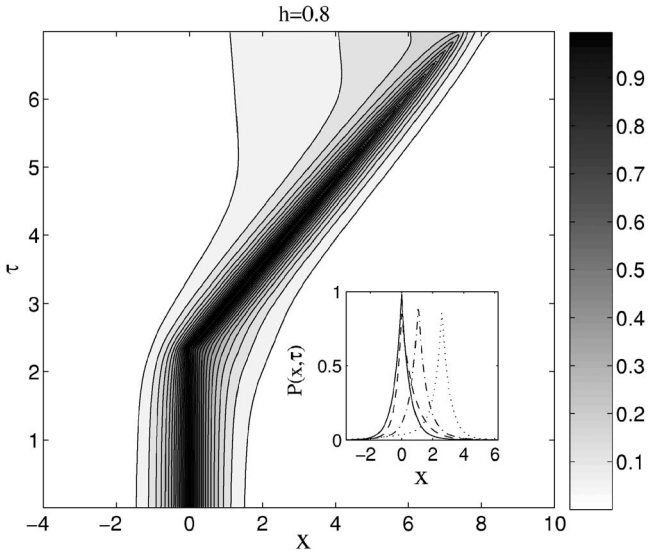

FIG. 3. Contour plot for the probability density distribution of the line defect for a scratch everywhere below the critical tilt angle: pinned regime. The darker areas correspond to higher probability. The tilt of the upper segment of the defect is $h=0.8<h_c=1$, the cusp is at $\tau_1=7/3\approx 2.33$ and the total length of the sample is $L_\tau=7$. The inset shows the probability density distribution for $\tau=1$ solid line, $\tau=2.33$ dashed line, $\tau=3$ dashed-dotted line, $\tau=4$ dotted line. Note that the distribution, while remaining localized, develops an asymmetry for $\tau>7/3$.

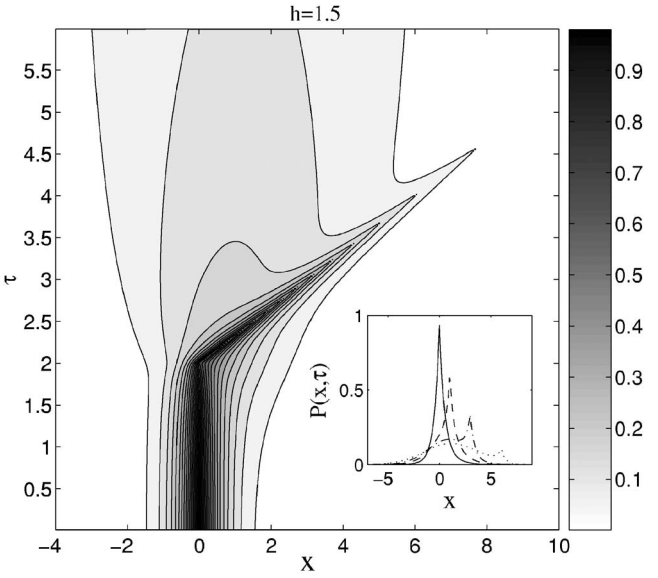

FIG. 4. Contour plot for the probability density distribution of the defect line whose upper part is above the critical tilt angle for the scratch: depinned regime. The tilt of the upper segment of the defect now is $h=1.5>h_c=1$, while $\tau_1=2$ and $L_\tau=6$. The inset shows the probability density distribution for $\tau=1$ solid line, $\tau=2.33$ dashed line, $\tau=3$ dashed-dotted line, $\tau=4$ dotted line. Note that the probability distribution begins to delocalize for $\tau>\tau_1=2$.

$$P(x,\tau)=\frac{1}{\mathcal{Z}}\int\int dy dy' \mathcal{Z}_t[y,L_\tau;y',\tau_1;h]\mathcal{Z}_t[y',\tau_1;x,\tau;0] \times e^{-|x|}e^{\tau} \quad (\tau<\tau_1). \tag{16}$$

Although the y integration can be computed analytically (see Appendix), we have resorted to numerical integration to handle the integration over y'.

Upon following a similar procedure for $\tau>\tau_1$, we obtain

$$P(x,\tau)=\frac{1}{\mathcal{Z}}\int \mathrm{d}y \mathcal{Z}_t[y,L_\tau;x-x_0(\tau),\tau;h]\int \mathrm{d}y' \mathcal{Z}_t[x-x_0(\tau),\tau;y',\tau_1;h]e^{-|y'|}e^{\tau_1} \quad (\tau>\tau_1). \tag{17}$$

As shown in the Appendix , in this case both the integrals can be done analytically.

Having now computed $P(x,\tau)$ for all imaginary times, we can examine the flux line probability distribution for this simple realization of an attractive line defect that suddenly changes direction. We have studied two cases, one where the tilt of the upper segment of the defect is below the critical value $h_c=1$ for delocalization (Fig. 3) and one where it is above (Fig. 4).

Note the following. For timelike coordinates below the kink at τ_1, the probability density does not differ much from the ground state probability density of Ref. 5, $P(x,\tau)=e^{-2|x|}$. However, as the position τ_1 of the kink in the scratch is approached from below, there is a broadening of the probability density on the right or "concave" side of the defect, and a similar narrowing on the left or "convex" (see Fig. 3). This phenomenon is not directly related to the delocalization of the flux line that occurs for tilts greater than the critical tilt, because it is present for both $h>1$ and $h<1$ (recall that the critical tilt is $h_c=1$). For $h<1$, after this small shifting of the probability density in the vicinity of the kink, the probability again resumes the ground state distribution. When $\tau\lesssim L_\tau$ we notice a small broadening of the probability which is a boundary condition effect.

When the tilt of the second segment of the defect is above the critical tilt $h_c=1$ (see Fig. 4), the probability density remains localized around the defect only for some small distance above the kink. Two local maxima of probability density appear, one localized on the defect and the other representing an approximately Gaussian probability distribution. As we move further away from the kink, the probability of observing the flux line close to the defect reduces, and the weight associated with the delocalizing diffusive part increases.

To better understand the depinning transition as the slope of the kink angle approaches the critical value h_c from below, we have computed the average position of the fluctuating line $\langle x\rangle_\tau=\int dx x P(x,\tau)$ for several tilts and sample lengths. In Fig. 5 we have plotted the average position of the fluctuating vortex line for several total lengths in the imaginary time direction L_τ. The position of the kink is held fixed at $\tau_1=2$ and the tilt is $h=0.8$. We observe that as L_τ grows, the distance m of the exit point of the vortex line $\langle x\rangle_{L_\tau}$ from the defect, indicated in the figure, tends to a constant. We have computed

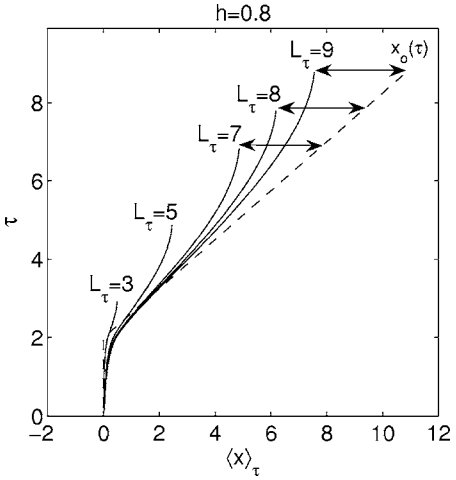

FIG. 5. Average position of the vortex $\langle x\rangle_\tau$: pinned regime. Here $\tau_1=2$ and $h=0.8$. The dashed line is the scratch trajectory and the solid lines represent the thermal average $\langle x\rangle_\tau$ for different sample lengths. The arrows mark the average distance of the step from the exit point of the scratch. As L_τ increases, this distance approaches a constant shift in the trajectory.

$$m(h) \equiv \lim_{L_\tau\to\infty}[\langle x\rangle_{L_\tau} - x_0(L_\tau)], \quad h<1, \tag{18}$$

by obtaining values for up to $L_\tau=50$ and then extrapolating L_τ to infinity. The convergence becomes very slow as $h\to 1^-$. The limiting offset $m(h)$ serves as an indicator of the depinning transition for $h\to h_c^-$. Similarly, for $h>1$, as can be seen from Fig. 6, a corresponding indicator is the offset of $\langle x\rangle_{L_\tau}$ from the origin, i.e., the original location of the defect. We now measure a shift

$$\tilde{m}(h) \equiv \lim_{L_\tau\to\infty}[\langle x\rangle_{L_\tau} - x_0(0)], \quad h>1, \tag{19}$$

which contributes to the total magnetization, in the vortex line case. By a fitting of $m(h)$ and $\tilde{m}(h)$ to $1/|h-1|^\nu$ (see Fig. 7) we find the critical exponent of the delocalization transition to be $\nu=1.0$.[18] An identical exponent describes the delocalization transition studied in Ref. 5.

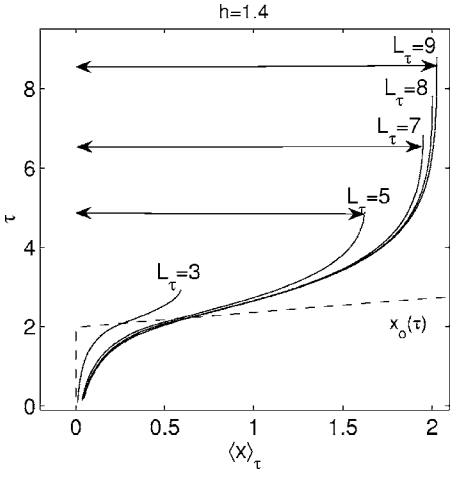

FIG. 6. Average position of the vortex $\langle x\rangle_\tau$: depinned regime. Here $\tau_1=2$ and $h=1.4$. The arrows represent the deflection of the vortex trajectory due to the tilted scratch and the dashed line is again the defect trajectory. $\langle x\rangle_{L_\tau}$ converges to ~ 2.2 as L_τ increases.

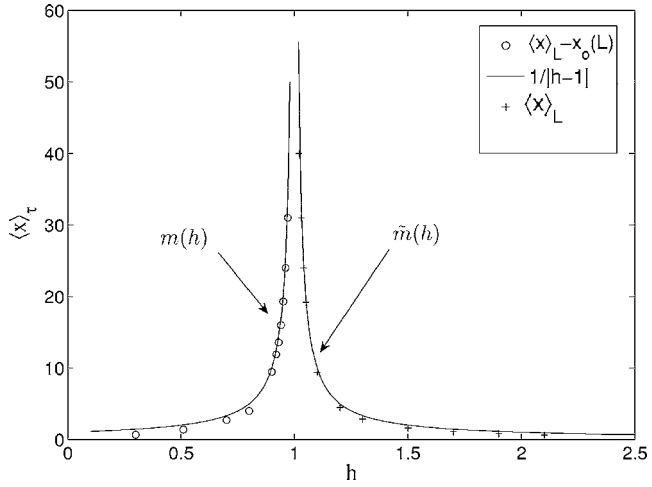

FIG. 7. Shift in the line trajectory near the depinning transition; curve to the left of $h_c=1$ represents $m(h)$ while that to the right represents $\tilde{m}(h)$.

IV. SOLUTION FOR A RANDOM TRAJECTORY IN THE ADIABATIC LIMIT

In this section we use the time dependent perturbation theory developed in Mostafazadeh[14] to analytically study the case of a slowly bending defect, i.e., $|\frac{dh}{d\tau}| \ll 1$. We will compute the probability distribution defined by Eq. (11), assuming that the initial and final states are the ground state, which should be a good approximation for physical systems with $h=$const for τ everywhere outside the interval $(0, L_\tau)$. As in Sec. II, we will preform a defect coordinate transformation

$$x \to x + x_0(\tau) \tag{20}$$

and reduce the problem to a straight defect in a time dependent external tilt field.

We will assume that $|h(\tau)|<1$. For any fixed $h(\tau)$ we can then be sure of the existence of a bound state. We suppose for the moment that $L_x<\infty$, which allows us to consider a *discrete* spectrum of free states. We can then write the matrix element of the time evolution operator as a product over time slices:

$$\langle x|S(\tau,0)|\psi_g\rangle = \lim_{N\to\infty}\sum_{\psi_1,\ldots,\psi_N} e^{-\Sigma_{j=0}^N E_{\psi_j}(t_j)\epsilon}\prod_{k=1}^N \langle x|\psi_N(\tau)\rangle_R \times {}_L\langle\psi_k(t_k)|\psi_{k-1}(t_{k-1})\rangle_R,$$

where $\epsilon\equiv\tau/N$, $t_k=k\epsilon$ and $|\psi_k(t_k)\rangle_R$ and ${}_L\langle\psi_k(t_k)|$ are, respectively, the instantaneous right and left eigenstates of $\mathcal{H}(\tau)$ for $h=h(\tau=t_N)$, namely,

$$\mathcal{H}(\tau)|\psi_k(t_k)\rangle_R = E_{\psi_k}(t_k)|\psi_k(t_k)\rangle_R. \tag{21}$$

Each of the summations embodied in $\Sigma_{\psi_1,\psi_2,\ldots,\psi_N}$ runs over the entire spectrum, while $|\psi_0(0)\rangle_R \equiv |\psi_g(0)\rangle_R$.

In the limit $\epsilon \to 0$, we can expand $|\psi_{k-1}(t_k-\epsilon)\rangle_R$ as $|\psi_{k-1}(t_k-\epsilon)\rangle_R \simeq |\psi_{k-1}(t_k)\rangle_R - \epsilon \frac{d}{dt}|\psi_{k-1}(t_k)\rangle_R$, so

$$ {}_L\langle\psi_k(t_k)|\psi_{k-1}(t_{k-1})\rangle_R = \delta_{\psi_k,\psi_{k-1}} - \epsilon A_{\psi_k,\psi_{k-1}}(t_k) + O(\epsilon^2), \tag{22}$$

where

$$ A_{\psi_k,\psi_{k-1}}(t_k) \equiv \langle\psi_k(t_k)|\frac{d}{dt}|\psi_{k-1}(t_{k-1})\rangle_R. \tag{23}$$

To linear order in ϵ, we can rewrite Eq. (22) as a sum of two mutually excluding terms

$$ {}_L\langle\psi_k(t_k)|\psi_{k-1}(t_{k-1})\rangle_R = e^{-\epsilon A_{\psi_k,\psi_k}(t_k)}[\delta_{\psi_k,\psi_{k-1}} + \epsilon e^{\epsilon A_{\psi_k,\psi_k}(t_k)}(\delta_{\psi_k,\psi_{k-1}} - 1)A_{\psi_k,\psi_{k-1}}(t_k)] + O(\epsilon^2). \tag{24}$$

Upon inserting Eq. (24) back to the matrix element (21) and keeping terms only up to the first order in $|A_{\psi_i,\psi_j}|$ [which is small if $h(\tau)$ is slowly varying], we have

$$ \langle x|S(\tau,0)|\psi_g\rangle_R = e^{-\int_0^\tau dt[E_{\psi_g}(t)+A_{\psi_g,\psi_g}(t)]}\left(\langle x|\psi_g(\tau)\rangle_R - \sum_{\psi\neq\psi_g}\langle x|\psi(\tau)\rangle_R\int_0^\tau dt e^{-\int_t^\tau dt'\Delta E(t')}A_{\psi,\psi_g}(t)\right). \tag{25}$$

Similarly, the other matrix element in Eq. (11), ${}_L\langle\psi_g(L_\tau)|S(L_\tau,\tau)|x\rangle$, reads

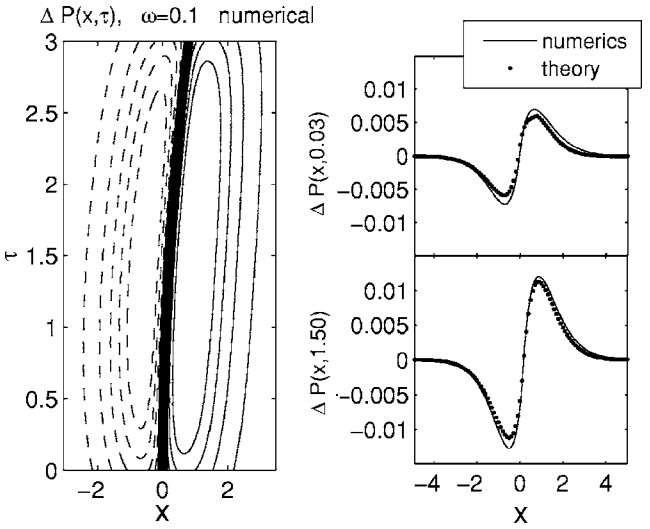

FIG. 8. Numerical solution $\Delta P(x,\tau)$ for a slowly moving defect. The thick solid line in the center represents the trajectory of the defect $x_0(\tau)=18[1-\cos(\omega\tau)]$, where $\omega=0.1$. The time domain shown corresponds to slightly less than 5% of a complete period. The dashed and solid lines are, respectively, negative and positive contours of the adiabatic correction $\Delta P(x,\tau)$. On the right: snapshots for times: $\tau=0.03$ and $\tau=1.50$ of $\Delta P(x,\tau)$ for both the analytic and the numerical solution.

$$ {}_L\langle\psi_g(L_\tau)|S(L_\tau,\tau)|x\rangle = e^{-\int_\tau^{L_\tau} dt[E_{\psi_g}(t)+A_{\psi_g,\psi_g}(t)]}\left({}_L\langle\psi_g(\tau)|x\rangle - \sum_{\psi\neq\psi_g}{}_L\langle\psi(\tau)|x\rangle\int_\tau^{L_\tau} dt e^{-\int_\tau^t dt'\Delta E(t')}A_{\psi_g,\psi}(t)\right), \tag{26}$$

where $\Delta E(t)\equiv E_\psi(t)-E_{\psi_g}(t)+A_{\psi,\psi}(t)-A_{\psi_g,\psi_g}(t)$. Upon sending L_x to infinity, the sum becomes an integral over wave vectors k and $\langle x|\psi_k(\tau)\rangle_R$ becomes the eigenstates tabulated in Eq. (A2) of the Appendix , with $h=h(\tau)$.

Provided $h(\tau)<1$, to zeroth order the probability density is independent of h, $P(x,\tau)\simeq e^{-2|x|}$. The lowest order adiabatic correction to the probability density $\Delta P(x,\tau)=P(x,\tau)-P_0(\tau)$ reads

$$\begin{aligned}\Delta P(x,\tau) &= e^{-|x|-h(\tau)x}\int\frac{dk}{2\pi(1+c)}\psi_{Lk}(x;h(\tau)) \times\int_\tau^{L_\tau} dt e^{-\int_\tau^t dt'\Delta E(t')}A_{\psi_k,\psi_g}(t) \\ &- e^{-|x|+h(\tau)x}\int\frac{dk}{2\pi(1+c)}\psi_{Rk}(x;h(\tau)) \times\int_0^{\tau} dt e^{-\int_t^\tau dt'\Delta E(t')}A_{\psi_k,\psi_g}(t),\end{aligned} \tag{27}$$

with $c=-\frac{1}{ik-h+1}$ (see Appendix). $\int\Delta P(x,\tau)dx=0$ and $P(x,\tau)$ is normalized to unity.

Upon substituting $x\to x-x_0(\tau)$ we can trivially transform back to a "moving defect" frame of reference. In this frame, the zeroth order term reads $P_0(\tau)=e^{-2|x-x_0(\tau)|}$.

To check the accuracy of this result, we have used the moving defect frame and numerically integrated the imaginary time Schrödinger equation for a slow sinusoidal defect trajectory $x_0(\tau)=18[1-\cos(0.1\tau)]$ with $L_\tau=3$ to obtain $\Delta P(x,\tau)=P(x,\tau)-e^{-2|x-x_0(\tau)|}$. The results are shown in Fig. 8.[19] On the right hand side of Fig. 8 we plotted two snapshots of the theoretical (lowest order correction) and numerical $\Delta P(x,\tau)$ for two different times. The agreement between the two results is fairly good, even for x and τ close to the boundaries. Note that the probability density piles up on the side of the radius of curvature, and is depleted on the opposite side.

However, the agreement deteriorates for rapidly changing defect trajectories. In Fig. 9 we have plotted the numerically evaluated $\Delta P(x,\tau)$ for $x_0(\tau)=3.6[1-\cos(0.5\tau)]$ with $L_\tau\simeq 6.3$ and compared with the analytical result. The three snapshots on the right indicate significant deviation from the theory in the center of the range of τ values, where $\frac{dx_0}{d\tau}$ is changing rapidly. Note from the more exact numerical solution that probability again piles up on the side of the radius of curvature.

V. CONCLUSIONS

In this paper we studied the interaction of a single vortex with a quenched meandering linear defect in a planar super-

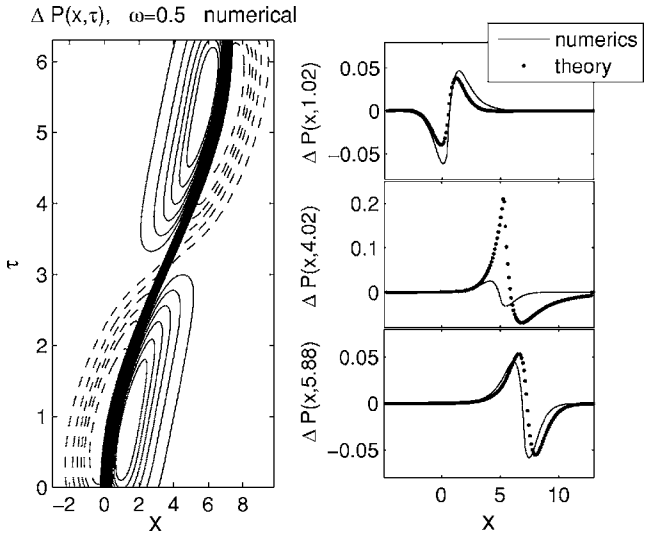

FIG. 9. Numerical solution $\Delta P(x,\tau)$ for a rapidly moving defect. The thick solid line in the center represents a half-period of the defect trajectory $x_0(\tau)=3.6[1-\cos(\omega\tau)]$, where $\omega=0.5$. The dashed and solid lines are, respectively, negative and positive contours of the adiabatic correction $\Delta P(x,\tau)$. On the right: snapshots for times: 1.02, 4.02, and 5.88 of our approximate solution of $\Delta P(x,\tau)$ compared with the numerical result.

conductor. We analytically calculated the partition function for the case of a straight defect and then used it to derive the probability density profile of a flux line interacting with a defect with a sudden change of direction, or "kink." We found that, in the vicinity of the kink, the vortex is more likely to be located on the concave side of the defect, and that a delocalization transition occurs when the relative angle between the externally applied magnetic field and the defect exceeds some critical value. As we numerically and, in the adiabatic limit, analytically verified, these conclusions are not restricted to piecewise straight defect trajectories.

We expect that some of our results can be tested in the laboratory. The simple kinked geometry (as described in Sec. III of this paper) could be experimentally realized by, for example, using an AFM tip to etch multiple defects on the surface of a thin superconducting slab, as shown in Fig. 10, introducing vortices by means of an in-plane magnetic field, and then measuring the transverse component of the in-plane magnetic field $\vec{b}_\perp$. In spite of the absence of an external transverse magnetic field, $\vec{b}_\perp$ can be nonzero due to the pinning of the vortex to the meandering defect. Since $b_\perp \sim \langle x\rangle_{L_\tau}-\langle x\rangle_0$, as seen in Figs. 5 and 6, the magnitude of $\vec{b}_\perp$ will depend on the specifics of the defect trajectory. By keeping the length of the sample L_τ and position of the kink τ_1 constant, and varying only the effective tilt h by using many samples with varying kink angles, one should observe $b_\perp$ reaching a maximum close to the predicted critical tilt. Bulk effects that facilitate measurements would arise from a dilute array of identical kinked defect trajectories, as in Fig. 10. To avoid the complicating effect of vortex-vortex interactions, the vortex array should be similarly dilute. The perpendicular field $\vec{b}_\perp$ can then be measured by means of the torque $T\sim\vec{B}\times\vec{H}$ that will be exerted on the slab and will tend to align $\vec{B}$ with $\vec{H}$.

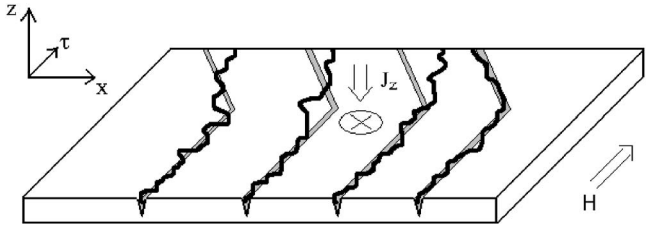

FIG. 10. Flux lines (represented by thick solid lines) penetrating through a thin superconducting slab where a series of similar linear defects have been etched. The critical value of the current J_z driven through the slab as shown, depends on the defect trajectories.

A setup of the type shown in Fig. 10 can also be used to measure the critical current. When the tilt h exceeds the critical value $h_c=1$, we expect a sharp decrease in J_c, as the vortices will in this case be only partially pinned, and more easily torn away from the defects by the Lorentz force.

A more direct method to test some of this paper's conclusions would be to use a Hall probe microscope to map the entering and exiting position of the flux line for different sample lengths and defect trajectories. An MFM tip could similarly be used to measure the force needed to move the vortex from its existing position—this force should show a marked increase when h becomes smaller than 1.

ACKNOWLEDGMENTS

We would like to thank M. Aziz, J. Blakely, G. Chan, V. Ignatesku, and E. Williams for useful conversations. This work was supported by the National Science Foundation through NSF Grant No. DMR-0231631 and the Harvard Materials Research Laboratory through NSF Grant No. NMR-0213805.

APPENDIX: ANALYTICAL COMPUTATION OF THE PROBABILITY DENSITY

In this Appendix we derive a number of results given in the main part of this paper. In most of what follows we assume that the lateral dimension of the planar superconductor L_x becomes infinite, although we shall be interested in the dependence of physical quantities on the size of the timelike dimension L_τ. All the quantities are given in the dimensionless units discussed in Sec. II.

1. Eigenstates of the Hamiltonian

The well known ground state of the Hamiltonian (7) with $h=0$ (in rescaled units) is simply $\psi_g(x)=e^{-|x|}$ with eigenenergy $E_g=-1$.[20] The odd and even parity extended eigenstates are, respectively, $\psi_k^{\rm odd}(x)\sim\frac{1}{\sqrt{1+k^2}}(k\cos kx-\sin k|x|)$ and $\psi_k^{\rm even}(x)\sim\sin kx$ with $E_k=k^2$ and k chosen to satisfy periodic boundary conditions in the x direction.

This complete set of eigenstates can be used in the expansion (8), the sum being turned into an integral as $L_x\to\infty$, which allows direct computation of the propagator. Provided

$|h|<1$, the case $h\neq 0$ can be reduced to $h=0$ via the "imaginary gauge transformation" $e^{hx}H(h)e^{-hx}=H(0)$. In this case, Eq. (10) can be obtained by straightforward evaluation of the integral

$$\mathcal{Z}_t[x,\tau;y,0;0] = e^{-|x|-|y|+\tau}+\frac{1}{\pi}\int_0^\infty dk e^{-k^2\tau} \times\left(\frac{(k\cos kx-\sin k|x|)(k\cos ky-\sin k|y|)}{1+k^2} + \sin kx\sin ky\right). \quad \text{(A1)}$$

Above the delocalization transition, the nature of the eigenstates changes and there is no longer a bound state. The non-Hermitian nature of the Hamiltonian (7) now becomes important. The right eigenstates for $h>0$ (Ref. 21) are (see Ref. 5):

$$\psi_{R^k}(x)\sim\begin{cases}e^{-ikx}+ce^{ikx-2hx} & \text{for } x>0,\\ (1+c)e^{-ikx} & \text{for } x<0,\end{cases} \quad \text{(A2)}$$

and the left ones

$$\psi_{L^k}(x)\sim\begin{cases}(1+c)e^{ikx} & \text{for } x>0,\\ e^{ikx}+ce^{-ikx+2hx} & \text{for } x<0\end{cases} \quad \text{(A3)}$$

with a common eigenenergy

$$E_k=k^2+2ihk \quad \text{(A4)}$$

and

$$c=-\frac{1}{ik-h+1}. \quad \text{(A5)}$$

The normalization condition is $\int dk|\psi_k\rangle_{RL}\langle\psi_k|=1$. Now the propagator is evaluated by computation of the integral $\int_{-\infty}^{\infty}dke^{-k^2\tau}\psi_{L^k}(x)\psi_{R^k}(x)$. Remarkably, the final result for the propagator is again Eq. (10).

2. Exact probability distribution of the fluctuating string

In this subsection we sketch details for obtaining results used in Sec. III. The y-integration in Eq. (16) can be computed analytically and is found to be

$$\int dy\,\mathcal{Z}_t[y,L_\tau;y',\tau_1;h]=1-\frac{e^{t-|y'|+hy'-h^2t}}{h^2-1}\operatorname{erfc}\left(\frac{|y'|}{2\sqrt{t}}-\sqrt{t}\right) -\frac{e^{hy'}}{2}\left[\frac{e^{h|y'|}}{1+h}\operatorname{erfc}\left(\frac{|y'|}{2\sqrt{t}}+h\sqrt{t}\right) +\frac{e^{-h|y'|}}{1-h}\operatorname{erfc}\left(\frac{|y'|}{2\sqrt{t}}-h\sqrt{t}\right)\right], \quad \text{(A6)}$$

where $t\equiv L_\tau-\tau_1$.

The y integration in Eq. (17) is formally the same as the integral (A6), τ_1 and y' having to be substituted with τ and $x-x_0(\tau)$, respectively. The y' integration is similarly found to be equal to

$$\int dy'\,\mathcal{Z}_t[X,\tau;y',\tau_1;h]e^{-|y'|} = Q(h,X,\tau-\tau_1)+Q(-h,-X,\tau-\tau_1), \quad \text{(A7)}$$

where $X\equiv x-x_0(\tau)$ and

$$Q(h,x,t)=\frac{1}{2}e^{(1-2h)t-x}\operatorname{erfc}\left(\frac{-x}{2\sqrt{t}}+(1-h)\sqrt{t}\right) +\frac{e^{-h^2t-hx}}{2(2-h)}\left[e^{t-|x|}\operatorname{erfc}\left(\frac{|y'|}{2\sqrt{t}}-h\sqrt{t}\right) +e^{(1-h)^2t+(1-h)|x|}\operatorname{erfc}\left(\frac{|x|}{2\sqrt{t}}+(1-h)\sqrt{t}\right)\right]. \quad \text{(A8)}$$

*Electronic address: katifori@fas.harvard.edu

[1] G. Blatter, M. V. Feigel'man, V. B. Geshkenbein, A. I. Larkin, and V. M. Vinokur, Rev. Mod. Phys. **66**, 1125 (1994).

[2] W. Hofstetter, I. Affleck, D. R. Nelson, and U. Schollwock, Europhys. Lett. **66**, 178 (2004).

[3] I. Affleck, W. Hofstetter, D. R. Nelson, and U. Schollwock, J. Stat. Mech.: Theory Exp. 10 (2004) P10003.

[4] H.-C. Jeong and E. D. Williams, Surf. Sci. Rep. **34**, 171 (1999).

[5] N. Hatano and D. R. Nelson, Phys. Rev. B **56**, 8651 (1997).

[6] D. S. Fisher, M. P. A. Fisher, and D. A. Huse, Phys. Rev. B **43**, 130 (1991).

[7] T. Hwa, D. R. Nelson, and V. M. Vinokur, Phys. Rev. B **48**, 1167 (1993).

[8] T. P. Devereaux, R. T. Scalettar, and G. T. Zimanyi, Phys. Rev. B **50**, 13625 (1994).

[9] D. Lee and J. Blakely, Surf. Sci. **445**, 32 (1999).

[10] T. Hwa, P. Le Doussal, D. R. Nelson, and V. M. Vinokur, Phys. Rev. Lett. **71**, 3545 (1993).

[11] P. L. Doussal and D. R. Nelson, Physica C **232**, 69 (1994).

[12] R. P. Feynman and A. R. Hibbs, *Quantum Mechanics and Path Integrals* (McGraw-Hill, New York, 1965).

[13] H. Kleinert, *Path Integrals in Quantum Mechanics, Statistics and Polymer Physics* (World Scientific, Singapore, 1995).

[14] A. Mostafazadeh, Phys. Rev. A **55**, 1653 (1997).

[15] E. Zeldov (private communication).

[16] E. Katifori and D. R. Nelson (unpublished).

[17] Returning to the original, tilted defect frame of reference, we see that $\mathcal{Z}\sim\exp[-x^2/4\tau]$ as expected from Eq. (13) for $V_0\to 0$.

[18] $\tilde{m}(h)$ is related to the trapping length introduced in Ref. 5 as a measure of the offset of the flux line from the average position it would assume without the defect (here that would be $\langle x\rangle_\tau=0$ because of the boundary condition) and the critical exponent

computed here agrees with the exponent analytically predicted there.

[19] The corresponding tilt field for this trajectory is $h(\tau) = 0.9 \sin(\omega\tau)$, since with our rescaled units $h(\tau) = \frac{1}{2}\frac{dx_0}{d\tau}$.

[20] See, for example, E. Merzbacher, *Quantum Mechanics* (Wiley, New York, 1998), Chap. 6.

[21] The $h < 0$ eigenstates can be derived by considering that $\mathcal{H}^\dagger(h) = \mathcal{H}(-h)$.